JOURNAL OF CHEMICAL INFORMATION AND MODELING

Article

pubs.acs.org/jcim

Computational Discovery and Experimental Validation of Inhibitors of the Human Intestinal Transporter OATP2B1

Natalia Khuri,[†,‡] Arik A. Zur,[‡,⊥] Matthias B. Wittwer,[‡,#] Lawrence Lin,[‡] Sook Wah Yee,[‡] Andrej Sali,[‡,§] and Kathleen M. Giacomini*[,‡,∥]

[†]Bioengineering Department, Stanford University, Stanford, California 94305, United States

[‡]Department of Bioengineering and Therapeutic Sciences and [∥]Institute for Human Genetics, University of California San Francisco, San Francisco, California 94143, United States

[§]Department of Pharmaceutical Chemistry and California Institute of Quantitative Biosciences (QB3), University of California San Francisco, San Francisco, California 94158, United States

Supporting Information

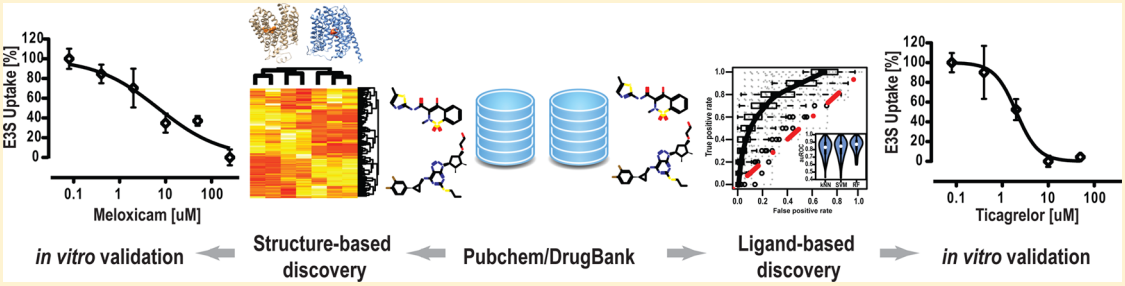

ABSTRACT: Human organic anion transporters (OATPs) are vital for the uptake and efflux of drugs and endogenous compounds. Current identification of inhibitors of these transporters is based on experimental screening. Virtual screening remains a challenge due to a lack of experimental three-dimensional protein structures. Here, we describe a workflow to identify inhibitors of the OATP2B1 transporter in the DrugBank library of over 5,000 drugs and druglike molecules. OATP member 2B1 transporter is highly expressed in the intestine, where it participates in oral absorption of drugs. Predictions from a Random forest classifier, prioritized by docking against multiple comparative protein structure models of OATP2B1, indicated that 33 of the 5,000 compounds were putative inhibitors of OATP2B1. Ten predicted inhibitors that are prescription drugs were tested experimentally in cells overexpressing the OATP2B1 transporter. Three of these ten were validated as potent inhibitors of estrone-3-sulfate uptake (defined as more than 50% inhibition at 20 μM) and tested in multiple concentrations to determine exact IC_{50}. The IC_{50} values of bicalutamide, ticagrelor, and meloxicam suggest that they might inhibit intestinal OATP2B1 at clinically relevant concentrations and therefore modulate the absorption of other concomitantly administered drugs.

INTRODUCTION

In humans, the number of different membrane proteins involved in the uptake and efflux of important substances, such as sugars, vitamins, toxins, signal molecules, and drugs, is relatively small compared to the large number of types of ligands. Thus, the structures of these proteins may have evolved to bind structurally diverse entities, leading to increased odds for interaction among different ligands. Organic Anion Transporting Polypeptide protein 2B1 (OATP2B1) is expressed in several tissues of pharmacological importance, such as blood brain barrier, liver, and intestine, as well as in tumors.[1−4] In humans, OATP2B1 is expressed along the entire human intestine.[5−7]

OATP2B1 transporters have been shown to facilitate drug permeability in the intestine and contribute to the oral absorption and bioavailability of drugs.[8,9] The culmination of multiple drug properties determines the intestinal absorption of a drug (e.g., solubility, passive permeability, interaction with metabolic enzymes or efflux transporters); however, for some drugs, the interaction with uptake transporter is a prominent factor. OATP2B1 transports a broad range of substrates including statins (e.g., fluvastatin, rosuvastatin, and atorvastatin),[10−12] beta adrenergic blocking agents (e.g., talinolol and celiprolol),[13,14] hormones such as estrone-3-sulfate (E3S),[7] bosentan,[15] fexofenadine,[16] aliskiren,[17] asunaprevir,[18] and glyburide.[19] OATP2B1 substrates overlap partially with that of other members of the OATP superfamily.[7] For some of these substrates the intestinal pharmacological relevance of OATP2B1 has been demonstrated *in vivo*. For example, OATP2B1-mediated drug−drug interactions have been shown to decrease the oral bioavailability of the beta-blockers talinolol and ticlopidine.[9,20,21] Similarly, reduced function of OATP2B1 due to genetic polymorphism was reported to decrease the

Received: November 28, 2016
Published: May 31, 2017

ACS Publications © 2017 American Chemical Society

DOI: 10.1021/acs.jcim.6b00720
J. Chem. Inf. Model. 2017, 57, 1402−1413

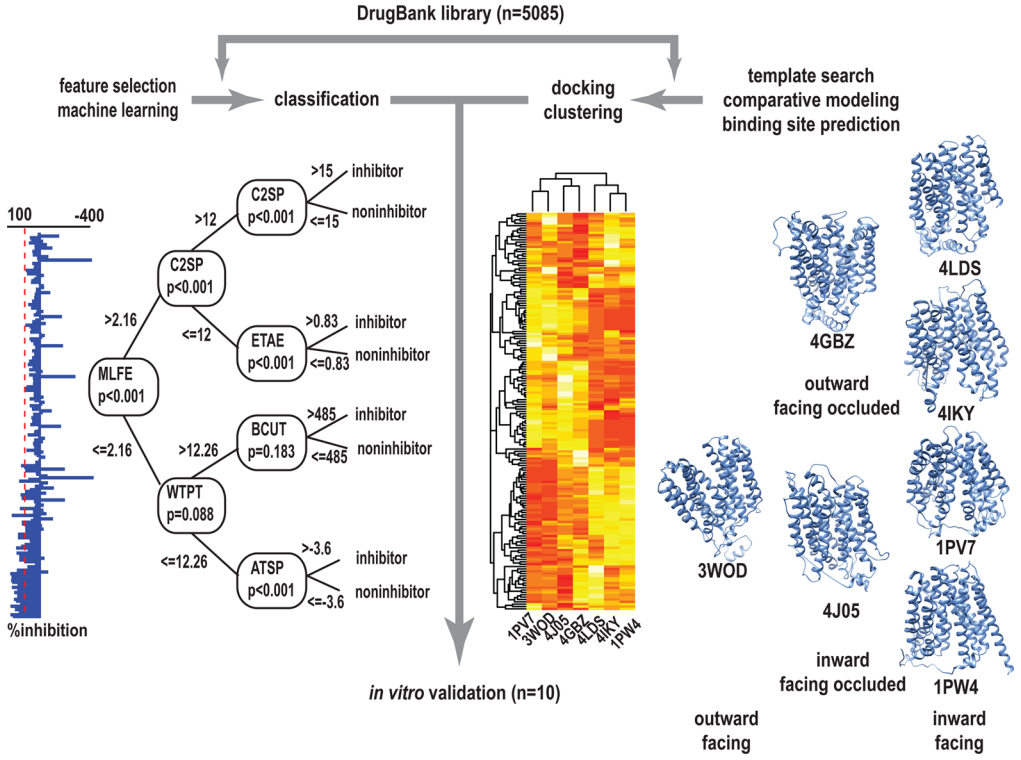

Figure 1. *In silico* OATP2B1 inhibitor discovery pipeline. Putative OATP2B1 inhibitors were predicted by docking the DrugBank library of 5805 compounds against seven comparative models of human OATP2B1 transporter in three different conformations and by classifying DrugBank compounds with the Random forest algorithm trained with known inhibitors and noninhibitors. Ten predicted inhibitors were selected for *in vitro* validation.

bioavailability of fexofenadine and midazolam.[22,23] Inhibition of intestinal OATP2B1 may also occur when high doses of fruit juice are ingested.[9,12,13]

OATP2B1 interaction with drugs may also be affected by its functional characteristics such as pH-dependent substrate transport mechanism.[24] For example, an acidic extracellular pH increases transport activity of OATP2B1 and broadens its substrate specificity.[25] Co-administered drugs may also affect OATP2B1 substrate interactions, and characterization of inhibitors is important for the optimization of oral drug delivery and the prediction of drug−drug interactions (DDIs). Today, transporter inhibition assays[26−43] are used with increased throughput and productivity due to the availability of fluorescent substrates and overexpressing cell lines, and, recently, 45 inhibitors of E3S uptake were identified by a small inhibition screen of 225 compounds against OATP2B1.[44] However, these experiments remain costly and time-consuming, and it is desirable to have a computational workflow to rapidly examine large chemical libraries to predict inhibitors of OATP2B1.

OATP2B1 belongs to the Solute Carrier Organic Anion (SLCO) subfamily of a larger Solute Carrier (SLC) family of membrane transport proteins.[45] Several *in silico* methods for predicting new ligands of human solute carrier transporters (SLCs) have been published.[34,46−59] In the virtual screening, large *in silico* libraries of compounds can be docked against experimentally determined models of transporter proteins to select the compounds based on their physicochemical complementarity to the putative binding site on the transporter.[34,46−53,58] In lieu of experimentally determined models, comparative models can be used for virtual screening. These screening pipelines require accurate homology models and known binding sites. Accurate modeling of human transporters is challenging because of the lack of suitable template structures and because these proteins change their conformation during the transport of their substrates. As an alternative, 2D and 3D physicochemical properties or pharmacophores important for the ligand's interaction with the transporter can be used to correlate *in vitro* activity with molecular properties.[35] However, ligand-based models tend to identify compounds structurally similar to those that were used for training or derivation of pharmacophores.

Both methods, structure- and ligand-based, require post-processing of the results from virtual screens, such as manual inspection and/or automated filtering based on predetermined properties, such as size, molecular weight, charge, and so on. In principle, predictions from both methods could be aggregated, thus eliminating the need for manual inspection of large number of predicted poses. In fact, there has been an increasing interest in combining ligand-based and structure-based approaches, with the aim of maximizing the accuracy, number, and diversity of predicted ligands.[60] Two alternative approaches, consensus ranking and complementary selection, are often used to integrate such predictions. Consensus ranking selects compounds that are top scoring by both methods, while complementary selection includes compounds that are top scoring by either method.[61] In this work, we use a consensus-ranking approach because it allows us to narrow down the list of predicted hits and avoid reranking the hits from two computational methods needed for complementary selection. Thus, the primary goal of this study was to identify new inhibitors of transport by human OATP2B1 transporter by finding overlapping predictions from ligand-based and structure-based virtual screens (Figure 1) and to validate

DOI: 10.1021/acs.jcim.6b00720
J. Chem. Inf. Model. 2017, 57, 1402−1413

predicted hits *in vitro* using inhibition of E3S uptake assay. Because the focus of this work is on identifying inhibitors among prescription drugs, the size of the *in silico* library used in this work is relatively small (~5,000 compounds), but the workflow could also be used with larger libraries.

MATERIALS AND METHODS

Data Preparation and Selection of an Algorithm for Binary Classification. The training data set was collected from the literature.[44] The data set contained inhibition values for 225 drugs and druglike compounds determined in an *in vitro* high throughput screen (HTS) against OATP2B1. E3S was used as a probe in the HTS. Forty-five compounds inhibited OATP2B1 transport of E3S by 50% or more[44] (Figure S1B). Compound names were mapped to PubChem molecular structure files. PaDEL software[62] and the *cxcalc* program in the ChemAxon (http://www.chemaxon.com) package were used to compute descriptors and molecular charge. Experimentally determined percent inhibition values[44] of the training compounds were converted to binary class labels, with '1' encoding percent inhibition value greater than or equal to 50% and '0', otherwise. Data set features, consisting of descriptors and charge, with zero variance were identified with function *nearZeroVar* in the *caret*[63] R package and removed. Pairwise descriptor correlations were computed to identify highly correlated features (correlation coefficient >0.95), and one randomly chosen feature was removed from each highly correlated pair. Feature reduction was then performed with the *cfs* filtering algorithm in the *FSelector* R package.[64] Three machine learning algorithms from the *caret* package in R, k-nearest Neighbors, Support Vector Machine, and Random forest, were employed to build binary classifiers with selected features. The *train* function in the *caret* R package was used to fit predictive models with default tuning parameters for the three algorithms. Area under the Receiver Operating Characteristic curve (auROC)[65] was used as the performance measure. A double loop 3-fold cross-validation[36] was used to access the predictive power of each algorithm. Double loop cross-validation was repeated 100 times, and the average auROC was computed to serve as a performance metric. The algorithm with the highest average auROC (Random forest) was selected for further modeling. Additionally, double loop cross-validation was repeated 100 times for each algorithm using all uncorrelated features with near zero variance. For each algorithm, distributions of 100 auROC values from the double-loop cross-validation with the reduced and full feature sets were assessed with the Student's *t* test in R. Finally, the Random forest algorithm was used to fit the entire training set and the 14 features; this final model was used in classifying DrugBank compounds as inhibitors and noninhibitors.

Comparative Modeling of the 3D Structures of OATP2B1. A search for suitable templates, multiple sequence alignment, and initial comparative modeling was performed using our online server ModWeb.[66] Predicted comparative models were manually examined, and models with charged helical residues facing the membrane were removed. Seven models (template PDB codes: 1PV7, 1PW4, 3WOD, 4GBZ, 4LDS, 4IKY, 4J05) were further refined as follows. A pairwise structure-to-sequence alignment was generated in PyMol, and predicted intracellular and extracellular loops were removed. The alignments were used to remodel OATP2B1 in different conformations with the default *automodel* protocol of MODELER-9v13[67,68] and SOAP-Protein score[69] as a metric. The model with the lowest SOAP-Protein score was retained. Putative binding sites on the comparative model were mapped using the FT-MAP server[70] with default settings. Next, OATP2B1 substrate, E3S, and 36 decoys were docked against predicted binding sites on comparative structure models. The models that discriminated (ranked highest) E3S from decoys were retained for further analysis.

Data Preparation and Classification of the DrugBank Library. Molecular structure files of compounds were downloaded from the DrugBank 3.0 database.[71] These compounds included FDA approved drugs and drug and endogenous metabolites. Descriptors and charge were computed using PaDEL and ChemAxon. Fourteen features identified by the feature section algorithm in the training step described above were retained, and the remaining 613 were ignored in further analyses. The entire DrugBank data set was classified into two groups, inhibitors and noninhibitors. The classification for each compound was made based on the prediction score, which ranged from 0 to 1. Compounds with the predicted score higher than a predetermined cutoff were classified as inhibitors.

Docking against Comparative Models. Predicted 3D poses of DrugBank compounds were downloaded from the ZINC database[72] and docked against the predicted binding site in each comparative model using a semiautomated docking protocol[73,74] implemented in DOCK 3.5.54.[75] For each compound, the best (lowest) scoring pose was identified, and the score of that pose was saved. The best scoring 500 compounds were saved for each comparative model.

Hit Selection. To prioritize candidate hits for an *in vitro* validation, an overlap between eight lists (i.e., RF-predicted inhibitors and seven docking scores' lists) was determined. Overlapping compounds were manually inspected to remove nondrugs.

Reagents. All reagents were obtained from Sigma-Aldrich (St. Louis, MI) and Santa Cruz Biotechnology (Santa Cruz, CA) and were of analytical grade with at least 95% purity, unless otherwise stated. All cell culture media and supplements were obtained from the Cell Culture Facility at the University of California, San Francisco, CA.

Cell Culture. Chinese hamster ovary (CHO) cells stably expressing OATP2B1 were a kind gift from Optivia Biotechnology, Inc. (Menlo Park, CA). CHO cells were grown in Dulbecco's Modified Eagle's Medium (DMEM, Cell Culture Facility, UCSF) substituted with 10% Foetal Bovine Serum (FBS, Cell Culture Facility, UCSF), 100 U/mL penicillin, 100 μg/mL streptomycin, 1% nonessential amino acids (NEAA), 2 mM L-glutamine, and 500 μg/mL Geneticin at 37 °C in a humidified atmosphere with 5% CO_2.

Inhibition Experiments with CHO-OATP2B1. CHO cells stably transfected with OATP2B1 were seeded at a density of 100,000 cells/mL in 24-well plates approximately 48 h prior to the experiments. On the day of the experiments, cells were washed with 0.5 mL of Hank's buffered salt solution (HBSS) per well and then preincubated for 10 min in 0.5 mL of HBSS per well. To assess inhibition, the cells were exposed to uptake buffer (0.1 μM unlabeled and 20 nM [^{3}H]-labeled estrone sulfate ([^{3}H]-E3S) in HBSS) containing either 20 μM or 200 μM inhibitor. Uptake of radioligand ([^{3}H]-E3S) was stopped after 3 min by washing twice with ice-cold HBSS. The cells were lyzed in 800 μL of lysis buffer (0.1 N NaOH and 0.1% SDS in bidistilled water) per well while shaking for 2 h. 650 μL of the lysate was then added to 3 mL of EcoLite scintillation fluid (MP Bio), and the radioactivity was determined on a

DOI: 10.1021/acs.jcim.6b00720
J. Chem. Inf. Model. 2017, 57, 1402−1413

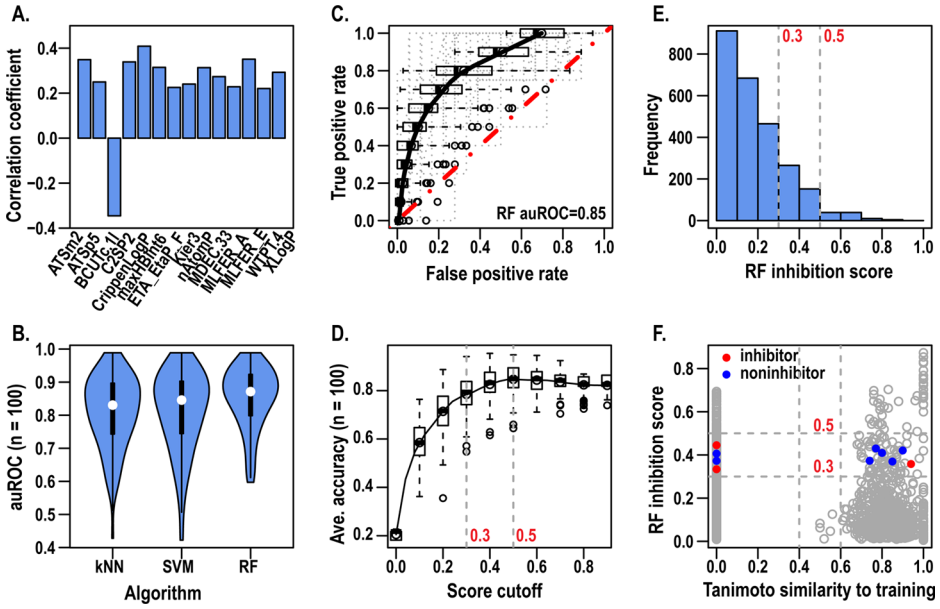

Figure 2. Results of feature selection, ligand-based modeling, and virtual screening of the DrugBank library. A. Fourteen most informative features derived from training data and their correlation with the inhibition values: Moreau-Broto autocorrelation descriptors using atomic weight (ATSm2) and polarizability (ATSp5), eigenvalue based descriptor noted for its utility in chemical diversity (BCUTc-11), carbon connectivity in terms of hybridization (C2SP2), atom-based LogP calculated using Crippen's approach (CrippenLogP), atom type electrotopological state (MaxHBint6), extended topochemical atoms (ETA_EtaP_F), Kappa shape index (Kier3), largest Pi system (nAtomP), molecular distance edge (MDEC.33), molecular linear free energy relations (MLFER_A and MLFER_E), weighted path (WTPT.4), and XLogP. B. Distribution of average auROCs for models built using three machine learning algorithms, k-nearest neighbors (kNN), Support Vector Machine (SVM), and Random forest (RF). C. Receiver Operating Characteristic (ROC) curve of 100 independent tests of binary RF classifiers. Average ROC curve is shown in black. ROC for a random classification is shown as a red dotted line. D. Distribution of accuracies in 100 independent tests of binary RF classifiers as a function of cutoff used in classification. Average accuracy is shown as a black solid line. Vertical gray dotted lines are drawn at cutoffs 0.3 and 0.5, respectively. E. Histogram of the number of predicted OATP2B1 inhibitors at different classification cutoffs. Vertical dotted lines are drawn at cutoffs 0.3 and 0.5, respectively. F. Plot of predicted inhibition scores for 5805 DrugBank compounds versus highest pairwise 2D Tanimoto similarity to training set. Each compound is shown as a circle. Compounds tested for inhibition *in vitro* are shown as filled circles: validated inhibitors are red and noninhibitors blue. Horizontal dotted lines are classification cutoffs (0.3 and 0.5), and the vertical dotted line is a pairwise 2D Tanimoto similarity cutoffs (0.4 and 0.6).

LS6500 Scintillation Counter (Beckman Coulter, Pasadena, CA). Values were corrected for protein concentration as determined with a BCA assay kit (Thermo Scientific, Rockford, IL). All values were determined in triplicate, and final values are expressed as % uptake relative to negative controls (1% dimethyl sulfoxide (DMSO)).

Determination of IC50 Values. CHO-OATP2B1 cells were seeded as described above. On the day of the experiments, cells were washed with 0.5 mL of Hank's buffered salt solution (HBSS) per well and then preincubated for 10 min in 0.5 mL of HBSS per well. To assess inhibition, the cells were exposed to uptake buffer (0.1 μM unlabeled and 20 nM [^{3}H]-labeled estrone sulfate in HBSS) containing increasing concentrations of inhibitor from 0.08 to 250 μM. Uptake was stopped after 3 min by washing twice with ice-cold HBSS. Radioactivity of samples was determined as described above. All values were determined in triplicate, and uptake was compared to positive (200 μM sulfobromophthalein (BSP)) and negative (1% DMSO) controls.

Pairwise Similarity Computation and Clustering. Two-dimensional Molecular ACCess System (MACCS), Extended Connectivity fingerprints (ECFP), and pairwise Tanimoto similarity coefficients were computed using MayaChemTools (http://www.mayachemtools.org). A default neighborhood radius of 2 was used to compute ECFP (ECFP2). Three-dimensional shape and feature similarity coefficients (Shape ST-Optimized, 10 configurations) were computed using the online PubChem Chemical Structure Clustering Tool[76] with default settings. Hierarchical compound clustering was performed in R using the *hclust* function of the *stats* library.[64]

RESULTS AND DISCUSSION

Binary Classification Model of OATP2B1 Inhibitors. Inhibition data of the E3S uptake by OATP2B1[44] were used to build a binary classification model. The data set (n = 225) was well diversified with the mean pairwise Tanimoto similarity coefficient (Tc) of 0.45 (Figure S1A). The reported inhibition values ranged from 100% (strong inhibitors) to −400% (putative activators) (Figure S1B). We computed 219 physicochemical and topological descriptors for all compounds in the training set and identified 14 important features with the highest weighted sum of information gain[77] metric. Among the selected descriptors, 13 correlated positively with reported inhibition values (Table S1). In contrast, a chemical diversity descriptor (BCUTc-11) was negatively correlated (Figure 2A), implying that inhibitors in the training set are chemically more similar to each other than noninhibitors. Interestingly, the feature selection algorithm (Material and Methods) retained two different estimates of compound's lipophilicity, Crippen-LogP and XLogP. These octanol/water partition coefficients positively correlated with inhibition, indicating that OATP2B1 inhibitors are more hydrophobic than noninhibitors. Although charge moderately correlated with inhibition (correlation coefficient r = −0.37; Table S1), we did not include it into

DOI: 10.1021/acs.jcim.6b00720
J. Chem. Inf. Model. 2017, 57, 1402−1413

the final selection because its computed information gain was zero.

Next, we used repeated retrospective 3-fold cross-validation to find the best performing binary classifier based on the 14 selected features, as follows. First, we partitioned 225 compounds into training (n = 180) and test sets (n = 45) by sampling known inhibitors and noninhibitors without replacement. Second, 3-fold cross-validation on the training data set was used to optimize binary classifiers. The predictive power of optimized classifier was assessed on the withheld test set. We tested three widely used machine learning algorithms, k-nearest neighbors (kNN),[78] Support Vector Machine (SVM),[79] and Random forest (RF).[80] The kNN algorithm is a simple similarity search technique and was used as a baseline for the comparison between algorithms. One hundred repeated iterations of data partitioning, model building, and model testing were performed for each algorithm; model assessment relied on the area under the Receiver Operating Characteristic (ROC) curves (auROCs). While all algorithms produced relatively accurate models, the most accurate classifiers (as judged by auROC) were built with the RF algorithm. The average auROC for RF classifiers was 0.85 ± 0.09, significantly higher than the average auROC values obtained with the kNN (auROC = 0.81 ± 0.11, Student's t test p-value = 0.003961) and SVM (auROC = 0.81 ± 0.12, Student's t test p-value = 0.008367) algorithms (Figure 2B and Figure S2). Additionally, the distribution of auROC values for RF classifiers had a shorter tail, indicating that there was less variability in RF predictions compared to predictions by kNN and SVM models (Figures 2B and 2C). The average accuracies for kNN and SVM classifiers were 0.82 and 0.83, respectively. The average accuracy of RF classifier was 0.85 (Table S2A).

Given the heuristic nature of feature selection, we tested its robustness by demonstrating that the 14 selected features performed as well as all 219 features (Table S2A). The kNN and RF models with the 14 features were more accurate than models built with all features, while the average auROC of the full-featured SVM models slightly increased from 0.81 to 0.84. These differences were not statistically significant in pairwise Student's t tests, thus justifying the use of the selected subset of molecular descriptors. Moreover, we did not see significant changes in overall accuracy, sensitivity, or specificity of classifiers with a reduced set of descriptors compared to classifiers built with all features (Tables S2A).

Binary classifiers output a score between 0 and 1, which can be used to classify compounds. A cutoff value for classification must be chosen to classify each compound as an inhibitor or noninhibitor. When a training set contains equal numbers of inhibitors and noninhibitors, a cutoff of 0.5 is typically used.[81] Because our training data set contained 45 inhibitors and 180 noninhibitors (Figure S1B), we determined the cutoff by maximizing the classification accuracy (i.e., percent of correctly classified test compounds; Figure 2D). For the RF algorithm, the highest classification accuracy of 84.9% is achieved incidentally at the cutoff of 0.5 and 0.78 at the cutoff of 0.3 (Tables S2A, B). For downstream analyses, we set the cutoff to 0.3 despite decreased classification accuracy. A binary classifier of OATP2B1 inhibitors and noninhibitors built using the partial least-squares projection to latent structures (PLS) algorithm was previously reported with an accuracy of 0.77 for a cutoff of 0.32.[44] Thus, our RF classifier has comparable performance. Additionally, decreasing cutoff for classification from 0.5 to 0.3 resulted in a significant increase in the RF classifier sensitivity (0.46 to 0.65) and a slight decrease in the classifier's specificity (from 0.96 to 0.81). For ligand-based virtual screening, a less stringent cutoff value would allow for identification of chemically novel inhibitors at the expense of a greater number of false positives, while a stringent cutoff would favor compounds similar to those in the training set and fewer false positives.[81]

Virtual Screening for OATP2B1 Inhibitors with the RF Classifier. Once the best-performing algorithm was identified, the full data set (n = 225) was used to build a final binary classification model (RF classifier, thereafter). We used the RF classifier to partition 5805 compounds in the DrugBank library[82] into two groups, inhibitors and noninhibitors. Ninety-two inhibitors were predicted using a stringent cutoff of 0.5, and 509 inhibitors were predicted with a less stringent cutoff of 0.3 (Figure 2E). Interestingly, predicted inhibitors clustered into two groups: compounds structurally similar to the training compounds (Tc greater or equal to 0.6) and putative structurally novel inhibitors, i.e., compounds with low similarity to the training set (Tc less than 0.4; Figure 2F). These results are interesting, because structurally novel compounds were identified at both RF cutoffs. These results could in part be attributed to the failure of the MACCS fingerprints to identify similar compounds. We used a different fingerprint, namely ECFP2, to compute Tanimoto similarity coefficients and again identified several predicted inhibitors in the group of compounds, which were structurally dissimilar from the training data set (Figure S4). Most classification-based workflows remove predictions that are outside of the model's applicability domain. Filtering is frequently done according to some similarity measure; for example, a Tc score to the closest training compound is often used to determine whether a test compound is inside or outside the applicability domain. In our case, such a protocol would remove all compounds with scores greater than the cutoffs and Tc values lower than 0.4, thus, eliminating the possibility of discovering structurally novel inhibitors. Instead, we determined the applicability domain for RF classifier by identifying compounds that favorably dock against binding sites of comparative OATP2B1 models. Our assumption is that some (but not all) compounds that inhibit OATP2B1-mediated transport should interact with the binding site within the translocation pore of the transporter. A possible shortcoming of our approach is the requirement that a predicted inhibitor must dock favorably against all seven models (conformations) of the transporter. It is possible that some of the compounds that were eliminated bind to one or a few of the conformations only and still inhibit the transport. Additionally, it is also possible that compounds that did not dock favorably to the binding sites bind to a different binding site on the transport and still inhibit the transport. Because the RF classifier was built from HTS data, the mechanism of inhibition could not be elucidated. These types of compounds will be missed in our workflow. Finally, because the predicted hits dock favorably against all conformations, a hypothesis can be made that these compounds not only are inhibiting OATP2B1-mediated transport but also are being transported by the protein. Our *in vitro* assay (Figure 3) does not distinguish between inhibitors and substrates of OATP2B1, and this hypothesis was not tested.

Virtual Screening of the DrugBank Library with OATP2B1 Comparative Structure Models. Structure-based virtual screening relies on the availability of high quality three-dimensional models of proteins. To date, however, no

DOI: 10.1021/acs.jcim.6b00720
J. Chem. Inf. Model. 2017, 57, 1402−1413

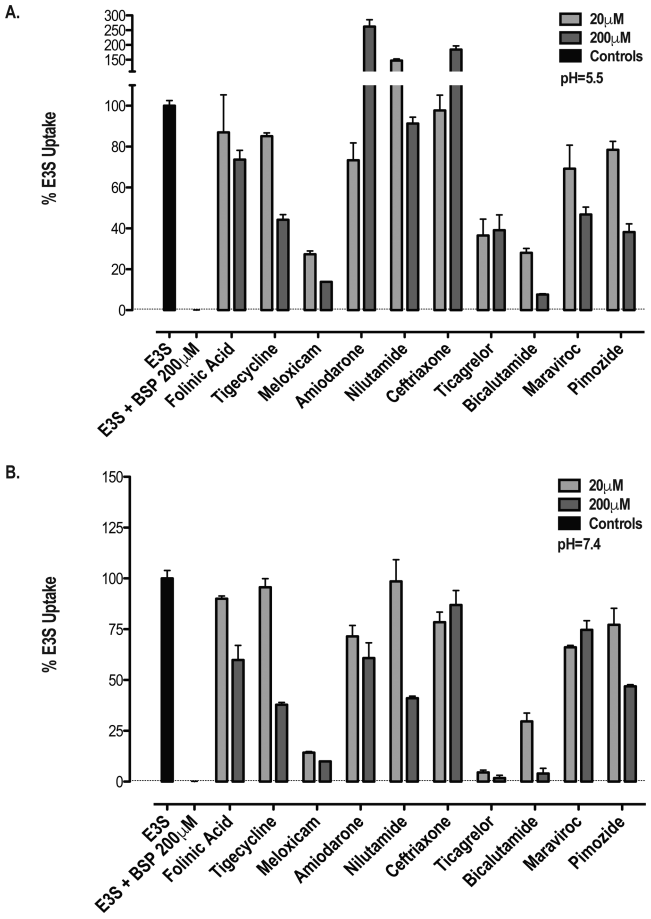

Figure 3. 2-Concentration inhibition of [^{3}H]-E3S uptake in human OATP2B1 overexpressing cells. Ten compounds were tested for inhibition of ^{3}H-E3S uptake (0.12 μM) in CHO-hOATP2B1 cells. Ten compounds predicted with the ligand-based approach and the structure-based approach were tested for inhibition at A. extracellular pH of 5.5 and B. extracellular pH of 7.4. Data are presented as percent uptake relative to controls (1% DMSO is 100% uptake and 200 μM BSP is 0% uptake controls). Inhibitor concentrations were 20 μM (light gray) and 200 μM (dark gray). Data are presented as mean ± standard deviation.

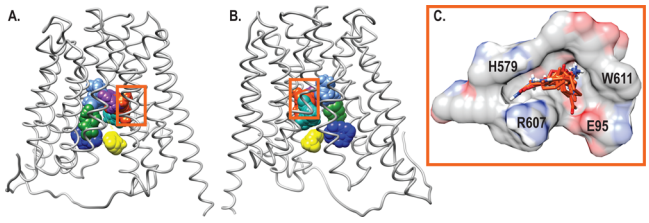

Figure 4. Results of binding site prediction for comparative models of human OATP2B1 transporter. A. Several predicted binding sites are shown as colored spheres on the representative comparative model built using the template structure in an inward-facing conformation (PDB code: 1PW4). The best scoring predicted binding site is shown in orange. B. An 180° rotation of the inward-facing comparative model and predicted binding pockets. C. Surface representation of the best scoring predicted binding site in an inward-facing conformation. Fragments docked using FTMap software are shown as orange sticks.

experimentally solved 3D structure of human OATP2B1 transporter has been published, and we built comparative models based on experimentally determined atomic structures of homologous Major Facilitator Superfamily (MFS)[83] proteins from prokaryotic and eukaryotic organisms. From the initial 18 models, we manually selected seven and refined them with Modeler-9v13[84,85] using the SOAP-Protein statistical potential.[86] Sequence identity between the templates and human OATP2B1 ranged from 11 to 20% (Supporting Information). Five models were based on inward-facing template structures, and two models were based on outward-facing templates (Figure S3), thus allowing us to probe ligand binding on both the intracellular and extracellular sides of the OATP2B1 transporter. We identified several putative binding sites for each comparative model using a fast fragment docking protocol[87] (Figures 4A and 4B). For final docking, the putative binding site with the highest density of docked fragments was selected (Supporting Information). Although the comparative models of OATP2B1 are low resolution and were built in a semi-automated fashion, several key features of the models provide information about the function of the protein. For example, the predicted positively charged pore of OATP2B1 is surrounded by transmembrane helices (TM) 2, 8, 9, and 10. The positively charged binding sites of the seven comparative models were structurally similar and included several backbone and side chain variations. Several residues in the predicted binding site might be important for interactions with ligands (e.g., Lys70, Glu95, His579, Arg607, and Trp611; Figure 4C). Positively charged residues in the binding site may contribute to the substrate specificity of OATP2B1 because its substrates are anionic. Among the 39 members of the OATP superfamily, a histidine residue is only found in OATP2B1 (Supporting Information). The protonation state of His579 may depend on the pH of the extracellular environment, because it is exposed to the solvent in the predicted outward-facing conformation, as previously noted.[88] Glu95 in the predicted TM2 is highly conserved among OATP superfamily members, and the corresponding glutamic acid residue (Glu74) in the hepatic homologue, OATP1B1, was critical for low concentration E3S uptake identified by alanine-scanning and site-directed mutagenesis.[89] The function of this residue in OATP2B1 is still unknown; it has been suggested that positively and negatively charged residues in the binding site of the OATP transporters form salt bridges to stabilize the binding site.[90]

We docked the DrugBank library, which includes all compounds from the training set, against each of the seven comparative models and determined whether inhibitors from the training set were found among the 500 top scoring compounds for each model. There were 92 compounds, which docked favorably against all seven comparative models, among them 25 out of 45 inhibitors from the training set. Thus, approximately 56% of known inhibitors were retrieved by our docking protocol. Overall, out of 45 known inhibitors, 33, 29, 34, 34, 29, 34, and 26 compounds docked favorably against comparative models built with templates 1PW4, 1PV7, 4LDS, 4IKY, 4GBZ, 3WDO, and 4J05, respectively. Not surprisingly, the smallest fraction of compounds docked against the comparative model in the inward-facing occluded state, namely 4J05. Several known OATP2B1 substrate drugs also docked favorably against all seven comparative models. These drugs were pitavastatin, rosuvastatin, pravastatin, fluvastatin, glyburide, taurocholic acid, and estrone sulfate. Three known substrates docked favorably against some but not all comparative models: fexofenadine, bosentan, and telmisartan. Additionally, we confirmed by docking against all comparative models, eight inhibitors, missing in our training data set:

DOI: 10.1021/acs.jcim.6b00720
J. Chem. Inf. Model. 2017, 57, 1402−1413

verlukast, rosiglitazone, gemfibrozil, silibinin B dihemisuccinate, repaglinide, estrone, simvastatin, and indinavir.

Thirty-three compounds out of 92 predicted docked inhibitors overlapped with the predictions of the Random forest classifier (RF cutoff = 0.3; Table S4). Our results show that several inhibitors predicted using our approach are positively charged, suggesting that it is also possible that Glu95 is directly involved in interactions with OATP2B1 inhibitors. Both positively charged residues in predicted binding sites, Lys70 and Arg607, participate in predicted interactions between OATP2B1 and favorably docked compounds. While Arg607 is involved in contacts with all predicted inhibitors, Lys70 is less frequently required for favorable docking. Both Lys70 and Arg607 are conserved among all members of OATP superfamily (Supporting Information). In OATP1B3, mutations of corresponding arginine residue (Arg580) for alanine and lysine resulted in reduced transport of sulfobromophthalein (BSP) and pravastatin.[91] Further experimental studies are needed to elucidate the role of these two residues in inhibition of OATP2B1-mediated transport of E3S. Finally, because of the low resolution of the comparative models and lack of experimental validation of these models, their main utility is to narrow down or prioritize the number of RF predictions while allowing for structural novelty.

We analyzed 9 physicochemical properties of three groups of predicted inhibitors. The first group included 33 predicted inhibitors that were identified by the combination of two methods, the second group consisted of 59 inhibitors predicted by docking, and the third group consisted of 59 inhibitors predicted by RF classifier only. These computed physicochemical properties were molecular weight and volume, SLogP, total polar surface area, and the number of rotatable bonds, hydrogen donors, acceptors, and heavy atoms. We also computed charge at pH 7.4. Interestingly, there was no statistical difference in all molecular properties, except molecular weight and volume, between the first two groups (i.e., inhibitors identified by docking alone and inhibitors identified by both methods). Compounds that were predicted by docking alone were smaller (p-value <0.005). Compounds that were predicted by RF classifier alone were bulkier and more hydrophobic (larger number of rotatable bonds, heavy atoms, higher LogP, and greater molecular weight and volume) than compounds in the first two groups (p-values <0.005). These results suggest a difference in the mechanism of inhibition between these groups.

***In Vitro* Validation of Hits.** Thirty-three predicted inhibitors were manually examined, and ten compounds were selected for an *in vitro* validation study with the criterion of a prescription drug currently used in the clinic (Table 1). These ten hits belong to diverse therapeutic classes: anticancer (bicalutamide, leucovorin, and nilutamide), anti-infectives (tigecycline, ceftriaxone, and maraviroc), antiarrhythmic (amiodarone), anticoagulant (ticagrelor), anti-inflammatory (meloxicam), and antipsychotic (pimozide) drugs. The maximal intestinal and plasma clinical concentrations of these ten compounds are listed in Table 1 as well as their classification scores. *In vitro* validation included testing for the extent of inhibition of [^{3}H]-E3S uptake by OATP2B1 at compound concentrations of 20 μM and 200 μM and in two extracellular pH conditions: pH 5.5 and pH 7.4. Three of the compounds, ticagrelor, meloxicam, and bicalutamide, potently inhibited OATP2B1 (i.e., more than 50% inhibition at 20 μM in both pH, where maximal inhibition is the uptake in the presence of 200 μM sulfobromophthalein (BSP)). Pimozide and tigecycline were less potent inhibitors and inhibited OATP2B1 by more than 50% only at 200 μM in both pHs. Nilutamide inhibited OATP2B1 by more than 50% at 200 μM at pH 7.4, and similarly maraviroc inhibited OATP2B1 at 200 μM but only at pH 5.5.

Table 1. Ten Hits from the DrugBank Library that are Predicted to Inhibit OATP2B1 by Both the Ligand-Based Approach and the Structure-Based Approach

compound	Tc	similarity to	oral dose (mg)[a]	$[I_2]$ intestinal max concn (μM)	$[I_1]$ plasma max concn (μM)
bicalutamide	0		50	464	1.96
tigecycline	0.92	tetracycline	NA	NA	2.48
maraviroc	0.77	valsartan	300	2336	1.20
pimozide	0		6	52	0.01
leucovorin	0.8	methotrexate	25	211	0.83
amiodarone	0		200	1239	4.34
nilutamide	0.74	flutamide	150	1891	26.80
ceftriaxone	0.85	cefamandole	NA	NA	463.48
meloxicam	0.94	piroxicam	15	170	2.56
ticagrelor	0		90	688	2.09

[a]FDA recommended oral dose. Tc: Tanimoto coefficient computed using MACCS fingerprints; represents the similarity score of predicted hits to the nearest training compound. $[I_2]$ is calculated as the oral dose divided by 250 mL. $[I_1]$ is the maximal plasma concentration reported in the Micromedex. NA marks not available data when the drug is not administered orally.

In this work, we aimed to discover new potent inhibitors of E3S transport by OATP2B1 using computational techniques. Combining two modeling techniques allowed us to reduce the total number of predicted hits and increase the success rate compared to published HTS. Results show that 30% of predicted OATP2B1 inhibitors inhibited E3S transport at 20 μM (Figure 3). This hit rate of 30% is higher than the hit rate of the published HTS against OATP2B1 (20% or 45 out of 225).[44] The observed 10% improvement suggests that classification models trained on previously published data may be valuable tools in ligand discovery. Due to the broad specificity and presence of multiple binding sites of OATP2B1, and the dependency of inhibition on the substrate used in the *in vitro* assay, it is challenging to assess computationally whether our method reduced false negatives. It is possible that some compounds labeled as negatives by either method could inhibit OATP2B1 transport of a different substrate or by binding at a different site on the transporter. We also show that by not limiting the applicability domain of RF classifier to compounds with similar physicochemical and topological features, we did, in fact, discover inhibitors that are structurally dissimilar from the drugs in the training data set. For instance, while meloxicam has a high similarity to a compound in the training data set (peroxicam, MACCS-based Tc = 0.78), ticagrelor and bicalutamide are structurally novel hits (Tc = 0).

Determination of IC_{50} Values for Selected Compounds. Half maximal inhibitory concentration (IC_{50}) was determined for 3 validated potent inhibitors (Figure 5). Ticagrelor, meloxicam, and bicalutamide, in particular, were tested to estimate the clinical relevance of OATP2B1 inhibition in the intestine. To estimate whether the IC_{50} values for ticagrelor, meloxicam, and bicalutamide (2.1, 1.6, and 12.9 μM) might be relevant clinically, we calculated the $[I_2]/IC_{50}$ ratio of

DOI: 10.1021/acs.jcim.6b00720
J. Chem. Inf. Model. 2017, 57, 1402−1413

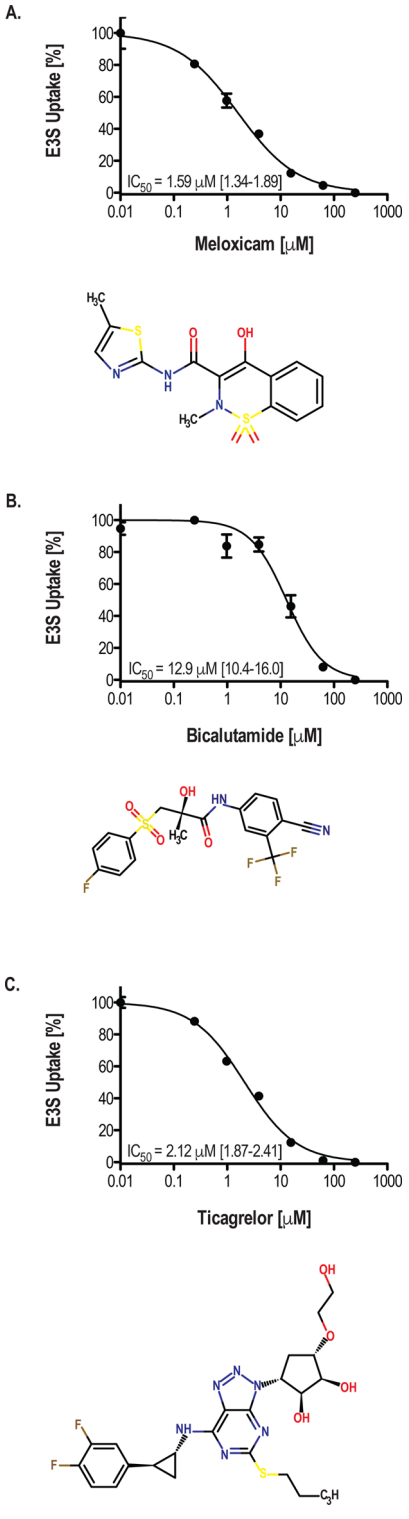

Figure 5. Results of IC_{50} determination for putative clinically relevant compounds. Inhibition of E3S uptake in CHO-hOATP2B1 cells was tested across a concentration range of 80 nM to 250 μM for three drugs: A. meloxicam, B. bicalutamide, and C. ticagrelor (each panel also presents the structure of the tested drug). Data are presented as percent uptake relative to controls (1% DMSO is 100% uptake and 200 μM BSP is 0% uptake controls). Data for each concentration tested are marked with a black circle and presented as mean ± standard deviation. Solid lines are nonlinear regression with a variable slope used to calculate the IC_{50}.

perpetrator drug concentration versus inhibition potency. The 2012 draft US Food and Drug Administration guidance (http://www.fda.gov) recommends a cutoff ratio value of higher than 10 for intestinal drug−drug interaction, where I_2 is defined as the estimated drug concentration in the intestinal milieu after oral administration of a single standard dose (90, 15, and 50 mg, respectively) divided by a volume of 250 mL.[92] The resulting concentrations for ticagrelor, meloxicam, and bicalutamide were 688, 170, and 464 μM, respectively, and the $[I_2]/IC_{50}$ ratios are 328, 106, and 36, respectively. Therefore, all three compounds may lead to significant inhibition of OATP2B1 transport in the intestine, potentially causing drug−drug interactions. Meloxicam is a nonsteroidal anti-inflammatory drug used to treat arthritis, a chronic disease with high prevalence in geriatric patients who also take other medications. For example, when meloxicam is coadministered with OATP2B1 substrates, such as statins, it may decrease the absorption and efficacy of statins. Ticagrelor is an adenosine diphosphate (ADP) receptor antagonist used as an anticoagulant in the case of coronary thrombosis, and many of the patients with coronary heart disease also require beta blocker treatment to reduce blood pressure or heart rate, thus potentially suffering from a drug−drug interaction. Bicalutamide is mostly used in anticancer treatments, where patients' comedication profile varies and the risk of a DDI should be evaluated individually.

CONCLUSION

In human, the organic anion transporting proteins are members of the OATP superfamily that mediate sodium-independent transport of structurally diverse amphipathic compounds, such as hormones, bile salts, toxins, and different drugs.[93] In comparison to the hepatic superfamily members, OATP1B1 and OATP1B3, the chemical space of compounds that interact with the intestinal OATP2B1 remains relatively unexplored.[7,44] Understanding the molecular features that regulate the flux of molecules through OATP2B1 is likely to facilitate design of orally available drugs. Virtual screening against human transporters remains challenging due to lack of experimentally determined atomic models of these proteins. To overcome this challenge, we developed a workflow that integrates predictions from a machine-learning classifier and docking against several low-resolution comparative models. We screened a virtual library with a Random forest classifier and docking against multiple comparative models and identified new inhibitors of OATP2B1-mediated E3S. We validated predicted hits *in vitro*. Three out of ten predicted inhibitors were validated as potent inhibitors of OATP2B1, suggesting that the workflow can output useful predictions. Among the predicted three inhibitors, two compounds were structurally novel. Moreover, the IC_{50} values of bicalutimide, ticagrelor, and meloxicam suggest that they might inhibit intestinal OATP2B1 at clinically relevant concentrations and therefore modulate the absorption of concomitantly administered drugs.

ASSOCIATED CONTENT

Supporting Information

The Supporting Information is available free of charge on the ACS Publications website at DOI: 10.1021/acs.jcim.6b00720.

Training set diversity and inhibition activity, Figure S1; ROC curves for 100 independent test validation experiments, Figure S2; templates utilized for compara-

DOI: 10.1021/acs.jcim.6b00720
J. Chem. Inf. Model. 2017, 57, 1402−1413

tive structure modeling and two-way clustering of docking, Figure S3; plot of predicted inhibition scores for DrugBank compounds versus highest pairwise ECFP Tanimoto similarity to training set, Figure S4 (PDF)
Information gain of computed molecular descriptors and correlation between descriptor and inhibition values, Table S1; results of repeated cross-validation of ligand-based modeling of OATP2B1 inhibitors, Table S2; predicted inhibitors and their similarity to training set (Tanimoto coefficient), Table S3; similarity of DrugBank compounds to compounds in training data set, Table S4 (XLSX)

AUTHOR INFORMATION

Corresponding Author

*Phone: +1 415 476 1936. Fax: +1 415 514 4361. E-mail: kathy.giacomini@ucsf.edu. Corresponding author address: University of California San Francisco, 1550 4th Street, Box 2911, San Francisco, CA 94158, USA.

ORCID

Natalia Khuri: 0000-0001-9031-8124
Andrej Sali: 0000-0003-0435-6197
Kathleen M. Giacomini: 0000-0001-8041-5430

Present Addresses

[⊥]Department of Clinical Pharmacology and Pharmacometrics, Global Research and Development, Teva Pharmaceutical Industries, Netanya, Israel.
[#]Department of Research Pharmacokinetics, Bayer Pharma AG, Wuppertal, Germany.

Author Contributions

N.K. and A.A.Z. contributed equally.

Notes

The authors declare no competing financial interest.
Additional supporting research data of multiple sequence alignment of OATP2B1 and template sequences, PDB files of comparative models, and an SDF file of the DrugBank library for this article may be accessed at http://www.nataliakhuri.com/data/khuri-oatp2b1-2016.zip.

ACKNOWLEDGMENTS

This work has been supported by grants from the National Institutes of Health (R01 GM54762, U54 GM62529, P01 GM71790, and P01 A135707 to A.S.; U19 GM61390 and R01 GM117163 to K.M.G.; T32 GM008284 to N.K.) and from the US Food and Drug Administration (U01FD005978 to K.M.G). We are also grateful for computing hardware gifts from Mike Homer, Ron Conway, NetApp, IBM, Hewlett-Packard, and Intel.

ABBREVIATIONS

OATP2B1, Organic Anion Transporting Polypeptide 2B1; HTS, High Throughput Screen; RF, Random forest

REFERENCES

(1) Badee, J.; Achour, B.; Rostami-Hodjegan, A.; Galetin, A. Meta-Analysis of Expression of Hepatic Organic Anion-Transporting Polypeptide (Oatp) Transporters in Cellular Systems Relative to Human Liver Tissue. *Drug Metab. Dispos.* **2015**, *43*, 424−432.
(2) Oswald, S.; Groer, C.; Drozdzik, M.; Siegmund, W. Mass Spectrometry-Based Targeted Proteomics as a Tool to Elucidate the Expression and Function of Intestinal Drug Transporters. *AAPS J.* **2013**, *15*, 1128−1140.
(3) Wilhelm, M.; Schlegl, J.; Hahne, H.; Moghaddas Gholami, A.; Lieberenz, M.; Savitski, M.M.; Ziegler, E.; Butzmann, L.; Gessulat, S.; Marx, H.; Mathieson, T.; Lemeer, S.; Schnatbaum, K.; Reimer, U.; Wenschuh, H.; Mollenhauer, M.; Slotta-Huspenina, J.; Boese, J.H.; Bantscheff, M.; Gerstmair, A.; Faerber, F.; Kuster, B. Mass-Spectrometry-Based Draft of the Human Proteome. *Nature* **2014**, *509*, 582−587.
(4) Muller, J.; Keiser, M.; Drozdzik, M.; Oswald, S. Expression, Regulation and Function of Intestinal Drug Transporters: An Update. *Biol. Chem.* **2017**, *398*, 175−192.
(5) Thomas, V. H.; Bhattachar, S.; Hitchingham, L.; Zocharski, P.; Naath, M.; Surendran, N.; Stoner, C. L.; El-Kattan, A. The Road Map to Oral Bioavailability: An Industrial Perspective. *Expert Opin. Drug Metab. Toxicol.* **2006**, *2*, 591−608.
(6) Drozdzik, M.; Groer, C.; Penski, J.; Lapczuk, J.; Ostrowski, M.; Lai, Y.; Prasad, B.; Unadkat, J. D.; Siegmund, W.; Oswald, S. Protein Abundance of Clinically Relevant Multidrug Transporters Along the Entire Length of the Human Intestine. *Mol. Pharmaceutics* **2014**, *11*, 3547−3555.
(7) Kullak-Ublick, G. A.; Ismair, M. G.; Stieger, B.; Landmann, L.; Huber, R.; Pizzagalli, F.; Fattinger, K.; Meier, P. J.; Hagenbuch, B. Organic Anion-Transporting Polypeptide B (Oatp-B) and Its Functional Comparison with Three Other Oatps of Human Liver. *Gastroenterology* **2001**, *120*, 525−533.
(8) Shirasaka, Y.; Suzuki, K.; Shichiri, M.; Nakanishi, T.; Tamai, I. Intestinal Absorption of Hmg-Coa Reductase Inhibitor Pitavastatin Mediated by Organic Anion Transporting Polypeptide and P-Glycoprotein/Multidrug Resistance 1. *Drug Metab. Pharmacokinet.* **2011**, *26*, 171−179.
(9) Tamai, I. Oral Drug Delivery Utilizing Intestinal Oatp Transporters. *Adv. Drug Delivery Rev.* **2012**, *64*, 508−514.
(10) Grube, M.; Kock, K.; Oswald, S.; Draber, K.; Meissner, K.; Eckel, L.; Bohm, M.; Felix, S. B.; Vogelgesang, S.; Jedlitschky, G.; Siegmund, W.; Warzok, R.; Kroemer, H. K. Organic Anion Transporting Polypeptide 2b1 Is a High-Affinity Transporter for Atorvastatin and Is Expressed in the Human Heart. *Clin. Pharmacol. Ther.* **2006**, *80*, 607−620.
(11) Noe, J.; Portmann, R.; Brun, M. E.; Funk, C. Substrate-Dependent Drug-Drug Interactions between Gemfibrozil, Fluvastatin and Other Organic Anion-Transporting Peptide (Oatp) Substrates on Oatp1b1, Oatp2b1, and Oatp1b3. *Drug Metab. Dispos.* **2007**, *35*, 1308−1314.
(12) Kitamura, S.; Maeda, K.; Wang, Y.; Sugiyama, Y. Involvement of Multiple Transporters in the Hepatobiliary Transport of Rosuvastatin. *Drug Metab. Dispos.* **2008**, *36*, 2014−2023.
(13) Ieiri, I.; Doi, Y.; Maeda, K.; Sasaki, T.; Kimura, M.; Hirota, T.; Chiyoda, T.; Miyagawa, M.; Irie, S.; Iwasaki, K.; Sugiyama, Y. Microdosing Clinical Study: Pharmacokinetic, Pharmacogenomic (Slco2b1), and Interaction (Grapefruit Juice) Profiles of Celiprolol Following the Oral Microdose and Therapeutic Dose. *J. Clin. Pharmacol.* **2012**, *52*, 1078−1089.
(14) Shirasaka, Y.; Kuraoka, E.; Spahn-Langguth, H.; Nakanishi, T.; Langguth, P.; Tamai, I. Species Difference in the Effect of Grapefruit Juice on Intestinal Absorption of Talinolol between Human and Rat. *J. Pharmacol. Exp. Ther.* **2010**, *332*, 181−189.
(15) Treiber, A.; Schneiter, R.; Hausler, S.; Stieger, B. Bosentan Is a Substrate of Human Oatp1b1 and Oatp1b3: Inhibition of Hepatic Uptake as the Common Mechanism of Its Interactions with Cyclosporin a, Rifampicin, and Sildenafil. *Drug Metab. Dispos.* **2007**, *35*, 1400−1407.
(16) Akamine, Y.; Miura, M.; Komori, H.; Saito, S.; Kusuhara, H.; Tamai, I.; Ieiri, I.; Uno, T.; Yasui-Furukori, N. Effects of One-Time Apple Juice Ingestion on the Pharmacokinetics of Fexofenadine Enantiomers. *Eur. J. Clin. Pharmacol.* **2014**, *70*, 1087−1095.
(17) Vaidyanathan, S.; Camenisch, G.; Schuetz, H.; Reynolds, C.; Yeh, C. M.; Bizot, M. N.; Dieterich, H. A.; Howard, D.; Dole, W. P. Pharmacokinetics of the Oral Direct Renin Inhibitor Aliskiren in Combination with Digoxin, Atorvastatin, and Ketoconazole in Healthy

DOI: 10.1021/acs.jcim.6b00720
J. Chem. Inf. Model. 2017, 57, 1402−1413

Subjects: The Role of P-Glycoprotein in the Disposition of Aliskiren. *J. Clin. Pharmacol.* **2008**, *48*, 1323−1338.
(18) Eley, T.; Han, Y. H.; Huang, S. P.; He, B.; Li, W.; Bedford, W.; Stonier, M.; Gardiner, D.; Sims, K.; Rodrigues, A. D.; Bertz, R. J. Organic Anion Transporting Polypeptide-Mediated Transport of, and Inhibition by, Asunaprevir, an Inhibitor of Hepatitis C Virus Ns3 Protease. *Clin. Pharmacol. Ther.* **2015**, *97*, 159−166.
(19) Satoh, H.; Yamashita, F.; Tsujimoto, M.; Murakami, H.; Koyabu, N.; Ohtani, H.; Sawada, Y. Citrus Juices Inhibit the Function of Human Organic Anion-Transporting Polypeptide Oatp-B. *Drug Metab. Dispos.* **2005**, *33*, 518−523.
(20) Shirasaka, Y.; Suzuki, K.; Nakanishi, T.; Tamai, I. Intestinal Absorption of Hmg-Coa Reductase Inhibitor Pravastatin Mediated by Organic Anion Transporting Polypeptide. *Pharm. Res.* **2010**, *27*, 2141−2149.
(21) Tamai, I.; Nakanishi, T. Oatp Transporter-Mediated Drug Absorption and Interaction. *Curr. Opin. Pharmacol.* **2013**, *13*, 859−863.
(22) Imanaga, J.; Kotegawa, T.; Imai, H.; Tsutsumi, K.; Yoshizato, T.; Ohyama, T.; Shirasaka, Y.; Tamai, I.; Tateishi, T.; Ohashi, K. The Effects of the Slco2b1 C.1457c > T Polymorphism and Apple Juice on the Pharmacokinetics of Fexofenadine and Midazolam in Humans. *Pharmacogenet. Genomics* **2011**, *21*, 84−93.
(23) Nakanishi, T.; Tamai, I. Genetic Polymorphisms of Oatp Transporters and Their Impact on Intestinal Absorption and Hepatic Disposition of Drugs. *Drug Metab. Pharmacokinet.* **2012**, *27*, 106−121.
(24) Nozawa, T.; Imai, K.; Nezu, J.; Tsuji, A.; Tamai, I. Functional Characterization of Ph-Sensitive Organic Anion Transporting Polypeptide Oatp-B in Human. *J. Pharmacol. Exp. Ther.* **2004**, *308*, 438−445.
(25) Varma, M. V.; Rotter, C. J.; Chupka, J.; Whalen, K. M.; Duignan, D. B.; Feng, B.; Litchfield, J.; Goosen, T. C.; El-Kattan, A. F. Ph-Sensitive Interaction of Hmg-Coa Reductase Inhibitors (Statins) with Organic Anion Transporting Polypeptide 2b1. *Mol. Pharmaceutics* **2011**, *8*, 1303−1313.
(26) Hu, G.; Henke, A.; Karpowicz, R. J., Jr.; Sonders, M. S.; Farrimond, F.; Edwards, R.; Sulzer, D.; Sames, D. New Fluorescent Substrate Enables Quantitative and High-Throughput Examination of Vesicular Monoamine Transporter 2 (Vmat2). *ACS Chem. Biol.* **2013**, *8*, 1947−1954.
(27) Zhou, W.; Madrid, P.; Fluitt, A.; Stahl, A.; Xie, X. S. Development and Validation of a High-Throughput Screening Assay for Human Long-Chain Fatty Acid Transport Proteins 4 and 5. *J. Biomol. Screening* **2010**, *15*, 488−497.
(28) Sindelar, M.; Wanner, K. T. Library Screening by Means of Mass Spectrometry (Ms) Binding Assays-Exemplarily Demonstrated for a Pseudostatic Library Addressing Gamma-Aminobutyric Acid (Gaba) Transporter 1 (Gat1). *ChemMedChem* **2012**, *7*, 1678−1690.
(29) Zhang, L.; Nebane, N. M.; Wennerberg, K.; Li, Y.; Neubauer, V.; Hobrath, J. V.; McKellip, S.; Rasmussen, L.; Shindo, N.; Sosa, M.; Maddry, J. A.; Ananthan, S.; Piazza, G. A.; White, E. L.; Harsay, E. A High-Throughput Screen for Chemical Inhibitors of Exocytic Transport in Yeast. *ChemBioChem* **2010**, *11*, 1291−1301.
(30) Susa, M.; Choy, E.; Yang, C.; Schwab, J.; Mankin, H.; Hornicek, F.; Duan, Z. Multidrug Resistance Reversal Agent, Nsc77037, Identified with a Cell-Based Screening Assay. *J. Biomol. Screening* **2010**, *15*, 287−296.
(31) Badolo, L.; Rasmussen, L. M.; Hansen, H. R.; Sveigaard, C. Screening of Oatp1b1/3 and Oct1 Inhibitors in Cryopreserved Hepatocytes in Suspension. *Eur. J. Pharm. Sci.* **2010**, *40*, 282−288.
(32) Gui, C.; Obaidat, A.; Chaguturu, R.; Hagenbuch, B. Development of a Cell-Based High-Throughput Assay to Screen for Inhibitors of Organic Anion Transporting Polypeptides 1b1 and 1b3. *Curr. Chem. Genomics* **2010**, *4*, 1−8.
(33) Karaki, F.; Ohgane, K.; Fukuda, H.; Nakamura, M.; Dodo, K.; Hashimoto, Y. Structure-Activity Relationship Study of Non-Steroidal Npc1l1 Ligands Identified through Cell-Based Assay Using Pharmacological Chaperone Effect as a Readout. *Bioorg. Med. Chem.* **2014**, *22*, 3587−3609.
(34) De Bruyn, T.; van Westen, G. J.; Ijzerman, A. P.; Stieger, B.; de Witte, P.; Augustijns, P. F.; Annaert, P. P. Structure-Based Identification of Oatp1b1/3 Inhibitors. *Mol. Pharmacol.* **2013**, *83*, 1257−1267.
(35) Wittwer, M. B.; Zur, A. A.; Khuri, N.; Kido, Y.; Kosaka, A.; Zhang, X.; Morrissey, K. M.; Sali, A.; Huang, Y.; Giacomini, K. M. Discovery of Potent, Selective Multidrug and Toxin Extrusion Transporter 1 (Mate1, Slc47a1) Inhibitors through Prescription Drug Profiling and Computational Modeling. *J. Med. Chem.* **2013**, *56*, 781−795.
(36) Kido, Y.; Matsson, P.; Giacomini, K. M. Profiling of a Prescription Drug Library for Potential Renal Drug-Drug Interactions Mediated by the Organic Cation Transporter 2. *J. Med. Chem.* **2011**, *54*, 4548−4558.
(37) Esteva-Font, C.; Phuan, P. W.; Anderson, M. O.; Verkman, A. S. A Small Molecule Screen Identifies Selective Inhibitors of Urea Transporter Ut-A. *Chem. Biol.* **2013**, *20*, 1235−1244.
(38) Strouse, J. J.; Ivnitski-Steele, I.; Khawaja, H. M.; Perez, D.; Ricci, J.; Yao, T.; Weiner, W. S.; Schroeder, C. E.; Simpson, D. S.; Maki, B. E.; Li, K.; Golden, J. E.; Foutz, T. D.; Waller, A.; Evangelisti, A. M.; Young, S. M.; Chavez, S. E.; Garcia, M. J.; Ursu, O.; Bologa, C. G.; Carter, M. B.; Salas, V. M.; Gouveia, K.; Tegos, G. P.; Oprea, T. I.; Edwards, B. S.; Aube, J.; Larson, R. S.; Sklar, L. A. A Selective Atp-Binding Cassette Subfamily G Member 2 Efflux Inhibitor Revealed Via High-Throughput Flow Cytometry. *J. Biomol. Screening* **2013**, *18*, 26−38.
(39) Mohamed, T. M.; Zakeri, S. A.; Baudoin, F.; Wolf, M.; Oceandy, D.; Cartwright, E. J.; Gul, S.; Neyses, L. Optimisation and Validation of a High Throughput Screening Compatible Assay to Identify Inhibitors of the Plasma Membrane Calcium Atpase Pump–a Novel Therapeutic Target for Contraception and Malaria. *J. Pharm. Pharm. Sci.* **2013**, *16*, 217−230.
(40) Colton, C. K.; Kong, Q.; Lai, L.; Zhu, M. X.; Seyb, K. I.; Cuny, G. D.; Xian, J.; Glicksman, M. A.; Lin, C. L. Identification of Translational Activators of Glial Glutamate Transporter Eaat2 through Cell-Based High-Throughput Screening: An Approach to Prevent Excitotoxicity. *J. Biomol. Screening* **2010**, *15*, 653−662.
(41) Zhang, Y.; Byun, Y.; Ren, Y. R.; Liu, J. O.; Laterra, J.; Pomper, M. G. Identification of Inhibitors of Abcg2 by a Bioluminescence Imaging-Based High-Throughput Assay. *Cancer Res.* **2009**, *69*, 5867−5875.
(42) Gao, J.; Xu, Y.; Yang, Y.; Yang, Y.; Zheng, Z.; Jiang, W.; Hong, B.; Yan, X.; Si, S. Identification of Upregulators of Human Atp-Binding Cassette Transporter A1 Via High-Throughput Screening of a Synthetic and Natural Compound Library. *J. Biomol. Screening* **2008**, *13*, 648−656.
(43) Duan, P.; Li, S.; Ai, N.; Hu, L.; Welsh, W. J.; You, G. Potent Inhibitors of Human Organic Anion Transporters 1 and 3 from Clinical Drug Libraries: Discovery and Molecular Characterization. *Mol. Pharmaceutics* **2012**, *9*, 3340−3346.
(44) Karlgren, M.; Vildhede, A.; Norinder, U.; Wisniewski, J. R.; Kimoto, E.; Lai, Y.; Haglund, U.; Artursson, P. Classification of Inhibitors of Hepatic Organic Anion Transporting Polypeptides (Oatps): Influence of Protein Expression on Drug-Drug Interactions. *J. Med. Chem.* **2012**, *55*, 4740−4763.
(45) Hagenbuch, B.; Meier, P. J. Organic Anion Transporting Polypeptides of the Oatp/ Slc21 Family: Phylogenetic Classification as Oatp/ Slco Superfamily, New Nomenclature and Molecular/Functional Properties. *Pfluegers Arch.* **2004**, *447*, 653−665.
(46) Geier, E. G.; Schlessinger, A.; Fan, H.; Gable, J. E.; Irwin, J. J.; Sali, A.; Giacomini, K. M. Structure-Based Ligand Discovery for the Large-Neutral Amino Acid Transporter 1, Lat-1. *Proc. Natl. Acad. Sci. U. S. A.* **2013**, *110*, 5480−5485.
(47) Schlessinger, A.; Geier, E.; Fan, H.; Irwin, J. J.; Shoichet, B. K.; Giacomini, K. M.; Sali, A. Structure-Based Discovery of Prescription Drugs That Interact with the Norepinephrine Transporter. *Proc. Natl. Acad. Sci. U. S. A.* **2011**, *108*, 15810−15815.

DOI: 10.1021/acs.jcim.6b00720
J. Chem. Inf. Model. 2017, 57, 1402−1413

(48) Schlessinger, A.; Khuri, N.; Giacomini, K. M.; Sali, A. Molecular Modeling and Ligand Docking for Solute Carrier (Slc) Transporters. *Curr. Top. Med. Chem.* **2013**, *13*, 843−856.
(49) Schlessinger, A.; Wittwer, M. B.; Dahlin, A.; Khuri, N.; Bonomi, M.; Fan, H.; Giacomini, K. M.; Sali, A. High Selectivity of the Gamma-Aminobutyric Acid Transporter 2 (Gat-2, Slc6a13) Revealed by Structure-Based Approach. *J. Biol. Chem.* **2012**, *287*, 37745−37756.
(50) Chen, E. C.; Khuri, N.; Liang, X.; Stecula, A.; Chien, H. C.; Yee, S. W.; Huang, Y.; Sali, A.; Giacomini, K. M. Discovery of Competitive and Noncompetitive Ligands of the Organic Cation Transporter 1 (Oct1; Slc22a1). *J. Med. Chem.* **2017**, *60*, 2685−2696.
(51) Colas, C.; Grewer, C.; Otte, N. J.; Gameiro, A.; Albers, T.; Singh, K.; Shere, H.; Bonomi, M.; Holst, J.; Schlessinger, A. Ligand Discovery for the Alanine-Serine-Cysteine Transporter (Asct2, Slc1a5) from Homology Modeling and Virtual Screening. *PLoS Comput. Biol.* **2015**, *11*, e1004477.
(52) Colas, C.; Ung, P. M.; Schlessinger, A. Slc Transporters: Structure, Function, and Drug Discovery. *MedChemComm* **2016**, *7*, 1069−1081.
(53) George Thompson, A. M.; Ursu, O.; Babkin, P.; Iancu, C. V.; Whang, A.; Oprea, T. I.; Choe, J. Y. Discovery of a Specific Inhibitor of Human Glut5 by Virtual Screening and in Vitro Transport Evaluation. *Sci. Rep.* **2016**, *6*, 24240.
(54) Hansen, S. W.; Erichsen, M. N.; Fu, B.; Bjorn-Yoshimoto, W. E.; Abrahamsen, B.; Hansen, J. C.; Jensen, A. A.; Bunch, L. Identification of a New Class of Selective Excitatory Amino Acid Transporter Subtype 1 (Eaat1) Inhibitors Followed by a Structure-Activity Relationship Study. *J. Med. Chem.* **2016**, *59*, 8757−8770.
(55) Liu, H. C.; Goldenberg, A.; Chen, Y.; Lun, C.; Wu, W.; Bush, K. T.; Balac, N.; Rodriguez, P.; Abagyan, R.; Nigam, S. K. Molecular Properties of Drugs Interacting with Slc22 Transporters Oat1, Oat3, Oct1, and Oct2: A Machine-Learning Approach. *J. Pharmacol. Exp. Ther.* **2016**, *359*, 215−229.
(56) Ngo, T. D.; Tran, T. D.; Le, M. T.; Thai, K. M. Machine Learning-, Rule- and Pharmacophore-Based Classification on the Inhibition of P-Glycoprotein and Nora. *SAR QSAR Environ. Res.* **2016**, *27*, 747−780.
(57) Ose, A.; Toshimoto, K.; Ikeda, K.; Maeda, K.; Yoshida, S.; Yamashita, F.; Hashida, M.; Ishida, T.; Akiyama, Y.; Sugiyama, Y. Development of a Support Vector Machine-Based System to Predict Whether a Compound Is a Substrate of a Given Drug Transporter Using Its Chemical Structure. *J. Pharm. Sci.* **2016**, *105*, 2222−2230.
(58) Ung, P. M.; Song, W.; Cheng, L.; Zhao, X.; Hu, H.; Chen, L.; Schlessinger, A. Inhibitor Discovery for the Human Glut1 from Homology Modeling and Virtual Screening. *ACS Chem. Biol.* **2016**, *11*, 1908−1916.
(59) Zamora, I.; Winiwarter, S. Modeling Organic Anion-Transporting Polypeptide 1b1 Inhibition to Elucidate Interaction Risks in Early Drug Design. *J. Pharm. Sci.* **2016**, *105*, 3214−3220.
(60) Lavecchia, A.; Di Giovanni, C. Virtual Screening Strategies in Drug Discovery: A Critical Review. *Curr. Med. Chem.* **2013**, *20*, 2839−2860.
(61) Tan, L.; Geppert, H.; Sisay, M. T.; Gutschow, M.; Bajorath, J. Integrating Structure- and Ligand-Based Virtual Screening: Comparison of Individual, Parallel, and Fused Molecular Docking and Similarity Search Calculations on Multiple Targets. *ChemMedChem* **2008**, *3*, 1566−1571.
(62) Yap, C. W. Padel-Descriptor: An Open Source Software to Calculate Molecular Descriptors and Fingerprints. *J. Comput. Chem.* **2011**, *32*, 1466−1474.
(63) Kuhn, M. Building Predictive Models in R Using the Caret Package. *Journal of Statistical Software* **2008**, *28*, 1−26.
(64) R Development Core Team. *R: A Language and Environment for Statistical Computing*; 2012.
(65) Hanley, J. A.; McNeil, B.J. The Meaning and Use of the Area under a Receiver Operating Characteristic (Roc) Curve. *Radiology* **1982**, *143*, 29−36.
(66) Pieper, U.; Webb, B. M.; Dong, G. Q.; Schneidman-Duhovny, D.; Fan, H.; Kim, S. J.; Khuri, N.; Spill, Y. G.; Weinkam, P.; Hammel, M.; Tainer, J. A.; Nilges, M.; Sali, A. Modbase, a Database of Annotated Comparative Protein Structure Models and Associated Resources. *Nucleic Acids Res.* **2014**, *42*, D336−346.
(67) Webb, B.; Sali, A. Comparative Protein Structure Modeling Using Modeller. *Curr. Protoc Bioinformatics* **2014**, *47*, 5.6.1−5.6.32.
(68) Sali, A.; Blundell, T. L. Comparative Protein Modelling by Satisfaction of Spatial Restraints. *J. Mol. Biol.* **1993**, *234*, 779−815.
(69) Dong, G. Q.; Fan, H.; Schneidman-Duhovny, D.; Webb, B.; Sali, A. Optimized Atomic Statistical Potentials: Assessment of Protein Interfaces and Loops. *Bioinformatics* **2013**, *29*, 3158−3166.
(70) Brenke, R.; Kozakov, D.; Chuang, G.Y.; Beglov, D.; Hall, D.; Landon, M.R.; Mattos, C.; Vajda, S. Fragment-Based Identification of Druggable 'Hot Spots' of Proteins Using Fourier Domain Correlation Techniques. *Bioinformatics* **2009**, *25*, 621−627.
(71) Knox, C.; Law, V.; Jewison, T.; Liu, P.; Ly, S.; Frolkis, A.; Pon, A.; Banco, K.; Mak, C.; Neveu, V.; Djoumbou, Y.; Eisner, R.; Guo, A. C.; Wishart, D. S. Drugbank 3.0: A Comprehensive Resource for 'Omics' Research on Drugs. *Nucleic Acids Res.* **2011**, *39*, D1035−1041.
(72) Irwin, J. J.; Shoichet, B. K. Zinc−a Free Database of Commercially Available Compounds for Virtual Screening. *J. Chem. Inf. Model.* **2005**, *45*, 177−182.
(73) Huang, N.; Shoichet, B. K.; Irwin, J. J. Benchmarking Sets for Molecular Docking. *J. Med. Chem.* **2006**, *49*, 6789−6801.
(74) Fan, H.; Irwin, J. J.; Webb, B. M.; Klebe, G.; Shoichet, B. K.; Sali, A. Molecular Docking Screens Using Comparative Models of Proteins. *J. Chem. Inf. Model.* **2009**, *49*, 2512−2527.
(75) Mysinger, M. M.; Shoichet, B. K. Rapid Context-Dependent Ligand Desolvation in Molecular Docking. *J. Chem. Inf. Model.* **2010**, *50*, 1561−1573.
(76) Kaiser, J. Science Resources. Chemists Want Nih to Curtail Database. *Science* **2005**, *308*, 774a.
(77) Kullback, S.; Leibler, R. A. *Ann. Math. Stat.* **1951**, *22*, 79−86.
(78) Altman, N. S. An Introduction to Kernel and Nearest-Neighbor Nonparametric Regression. *Am. Stat.* **1992**, *46*, 175−185.
(79) Cortes, C.; Vapnik, V. Support-Vector Networks. *Mach. Learn.* **1995**, *20*, 273−297.
(80) Breiman, L. Random Forests. *Machine Learning* **2001**, *45*, 5−32.
(81) Freeman, E. A.; Moisen, G. G. A Comparison of the Performance of Threshold Criteria for Binary Classification in Terms of Predicted Prevalence and Kappa. *Ecol. Modell.* **2008**, *217*, 48−58.
(82) Knox, C.; Law, V.; Jewison, T.; Liu, P.; Ly, S.; Frolkis, A.; Pon, A.; Banco, K.; Mak, C.; Neveu, V.; Djoumbou, Y.; Eisner, R.; Guo, A. C.; Wishart, D. S. Drugbank 3.0: A Comprehensive Resource for 'Omics' Research on Drugs. *Nucleic Acids Res.* **2011**, *39*, D1035−D1041.
(83) Pao, S. S.; Paulsen, I. T.; Saier, M. H. Major Facilitator Superfamily. *Microbiology and Molecular Biology Reviews* **1998**, *62*, 1−34.
(84) Webb, B., Sali, A. Comparative Protein Structure Modeling Using Modeller. In *Current Protocols in Bioinformatics*; John Wiley & Sons, Inc.: 2002.
(85) Šali, A.; Blundell, T. L. Comparative Protein Modelling by Satisfaction of Spatial Restraints. *J. Mol. Biol.* **1993**, *234*, 779−815.
(86) Dong, G. Q.; Fan, H.; Schneidman-Duhovny, D.; Webb, B.; Sali, A. Optimized Atomic Statistical Potentials: Assessment of Protein Interfaces and Loops. *Bioinformatics* **2013**, *29*, 3158−3166.
(87) Brenke, R.; Kozakov, D.; Chuang, G.-Y.; Beglov, D.; Hall, D.; Landon, M. R.; Mattos, C.; Vajda, S. Fragment-Based Identification of Druggable 'Hot Spots' of Proteins Using Fourier Domain Correlation Techniques. *Bioinformatics* **2009**, *25*, 621−627.
(88) Leuthold, S.; Hagenbuch, B.; Mohebbi, N.; Wagner, C. A.; Meier, P. J.; Stieger, B. Mechanisms of Ph-Gradient Driven Transport Mediated by Organic Anion Polypeptide Transporters. *American Journal of Physiology - Cell Physiology* **2009**, *296*, C570.
(89) Li, N.; Hong, W.; Huang, H.; Lu, H.; Lin, G.; Hong, M. Identification of Amino Acids Essential for Estrone-3-Sulfate Transport within Transmembrane Domain 2 of Organic Anion Transporting Polypeptide 1b1. *PLoS One* **2012**, *7*, e36647.

DOI: 10.1021/acs.jcim.6b00720
J. Chem. Inf. Model. 2017, 57, 1402−1413

(90) Rizwan, A. N.; Krick, W.; Burckhardt, G. The Chloride Dependence of the Human Organic Anion Transporter 1 (Hoat1) Is Blunted by Mutation of a Single Amino Acid. *J. Biol. Chem.* **2007**, *282*, 13402−13409.
(91) Glaeser, H.; Mandery, K.; Sticht, H.; Fromm, M. F.; Konig, J. Relevance of Conserved Lysine and Arginine Residues in Transmembrane Helices for the Transport Activity of Organic Anion Transporting Polypeptide 1b3. *Br. J. Pharmacol.* **2010**, *159*, 698−708.
(92) Agarwal, S.; Arya, V.; Zhang, L. Review of P-Gp Inhibition Data in Recently Approved New Drug Applications: Utility of the Proposed [I(1)]/Ic(50) and [I(2)]/Ic(50) Criteria in the P-Gp Decision Tree. *J. Clin. Pharmacol.* **2013**, *53*, 228−233.
(93) Shitara, Y.; Maeda, K.; Ikejiri, K.; Yoshida, K.; Horie, T.; Sugiyama, Y. Clinical Significance of Organic Anion Transporting Polypeptides (Oatps) in Drug Disposition: Their Roles in Hepatic Clearance and Intestinal Absorption. *Biopharm. Drug Dispos.* **2013**, *34*, 45−78.

DOI: 10.1021/acs.jcim.6b00720
J. Chem. Inf. Model. 2017, 57, 1402−1413